Analysis of Acoustic Emission Pressure Test of Mortar Specimens with Different Materials

L. Pazdera[1,*], L. Topolar[1], R. Dvorak[1], M. Hodulakova[1]

[1] *Brno University of Technology, Faculty of Civil Engineering, Veveří 95, 602 00 Brno, Czech Republic*
[*] *pazdera.l@fce.vutbr.cz*

Abstract: The acoustic emission method is one of the tools for describing the behavior of a specimen during (mechanical) deformation. The compression test is one of the most conventional destructive methods for testing structural composites. Material engineers strive to find a compound with optimal properties. This paper aims to show the possibilities of a more detailed analysis of acoustic emission signals recorded during the loading of test specimens made from two different materials and two different sizes.

Keywords: accoustic emission; mortar; tensile; analysis; alkali activated.

1 Introduction

The main function of concrete elements in structures is the transmission of strength actions of loading when the concrete is exposed to various stresses. One of the most common building materials today is concrete. Its advantages include reasonable workability, good compressive strengths, durability, fire resistance and high heat accumulation. The traditional binder employed in its production has been Portland cement, whose production is not ideal from the environmental point of view. It is, however, relatively inexpensive. Additions of alkali-activated activators can result in the reduction of cement in the final mixture. The experiments discussed in this paper were conducted in order to compare an alkali-activated slag optimized in regard to chemical resistance with a conventional cement-based mortar. The experiment also studied the influence of specimen size on acoustic emission signals within the testing of prismatic strength [1, 2].

Compressive strength of concrete is a priority property of concrete or mortar for building construction. Compressive strength of concrete is the most important characteristic feature of concrete. The most commonly used is cubic compressive strength $f_{c,cube}$, which is determined on cubes. In our case, we used measurements of prismatic strength $f_{c,prism}$. Prismatic strength $f_{c,prism}$ is therefore measured on prism-shaped specimens. It is determined on prism-shaped specimens with the base to height ratio of 1:4 (1:3 is also allowed). Prismatic strength is lower than cubic strength $f_{c,cub}$:

$$f_{c,prism} = (0.7 \div 0.85) \times f_{c,cube}. \tag{1}$$

Since the aim of this paper is to monitor not only the resulting prismatic compressive strength, but also the behaviour of the specimens during loading, the acoustic emission method was selected to suit both tasks. There are not many methods that allow monitoring of changes in the structure of a material during loading. The acoustic emission method is based on the principle of recording acoustic responses inside a specimen using suitable sensors. Loading of a material results in formations of areas where the mechanical stress accumulates. Once this stress is released, e.g. a crack forms, a part of that energy is emitted in the form of a mechanical wave. The sensor then detects this wave. However, the recorded wave carries information not only about the source, but also about the path of the wave and the material the wave propagated through. Evaluation of the acoustic emission method is therefore far from a simple task [3–5].

2 Experimental set up

The experiment monitored the behaviour of test specimens with dimensions of 40 mm $\times$ 40 mm $\times$ 160 mm (marked as m) and 100 mm $\times$ 100 mm $\times$ 400 mm (marked as v) were. The specimens were designed of two

Tab. 1: Composition of the cement-based mixture

Component of mixture	Weight [g]
CEM III/A 32.5 R	1,000
Standardised sands	3,000
Water	450

Tab. 2: Composition of the mixture based on alkali-activated slag

Component of mixture	Weight [g]
Granulated Blast Furnace Slag	1,000
Stabdardised sands	3,000
Water	331.4
50% NaOH	113.8
Sodium water glass (M_s = 1.89)	93.9

different fine-grained mixtures, one based on cement (marked as c) and the other based on alkali-activated slag (marked as o). Loading of the specimens was on bases, i.e. 40 mm $\times$ 40 mm (1.6 $\times$ 10^3 mm^2) for the small specimens and 100 mm $\times$ 100 mm (10^4 mm^2) for the large specimens. The mixtures are in Tab. 1 and Tab. 2.

The specimens in the testing machine were loaded with a constantly increasing stress (0.6 MPa/s) until destruction. A photo of the testing machine is in Fig. 1b. Two acoustic emission sensors were placed on the specimens each time. The distance of the sensors from the end of the specimen was 10 cm. Both sensors were placed on the same surface of the specimen. The locations where the sensors were attached using beeswax are evident from Fig. 1a. Typical acoustic emission parameters, such as acoustic emission RMS, the number of hits over a specified acoustic emission level, etc., were detected every second, i.e. over a 0.6 MPa increase in the mechanical stress. Significant individual events were also recorded during loading [6,7].

3 Results

In the case of all the measurements, the monitored prismatic compressive strengths reached approximately identical average values, around 50 MPa. The cubic strength according to the Eq. (1) would then reach values in the range of 60 to 70 MPa.

Based on the information included in Tab. 3, it can be concluded that the influence of material composition on the velocity of longitudinal propagation is more evident in specimens from alkali-activated structures. Different propagation velocities can be observed for specimens of different sizes. In the case of cement specimens, the observed velocity is practically identical within the statistical error.

Fig. 2 presents the basic characteristics of the dependence of the acoustic emission Root Mean Square (RMS_{AE}) of the measured acoustic emission signals on the pressure stress (R). Thus, the RMS value was recorded and calculated at regular loading intervals.

Tab. 3: Wave propagation velocity.

Marked	Material	Volume [mm^3]	c [mm/µs]	R [MPa]
o-v	alcali activated	100 $\times$ 100 $\times$ 400	3.7	51
c-v	concrete	100 $\times$ 100 $\times$ 400	4.3	48
o-m	alcali activated	40 $\times$ 40 $\times$ 160	4.1	44
c-m	concrete	40 $\times$ 40 $\times$ 160	4.3	50

(a) Specimen, the arrows mark the placement of the acoustic emission sensors

(b) Placement of the specimen in the testing machine

Fig. 1: Specimen and experiment setup.

$$RMS_{AE} = \sqrt{\frac{\sum U_{AE}^2}{N}}, \tag{2}$$

where U_{AE} is the voltage at the acoustic emission sensor and N is the number of specimens during a stress change of 0.6 MPa, as stated in the measurement description. The graph in Fig. 2a incorporates a linear scale for RMS, while the graph in Fig. 2b incorporates a logarithmic resp. decibel scale.

$$RMS_{dB} = 20 \times \log_{10} \frac{U_{AE}}{U_{ref}}, \tag{3}$$

where U_{ref} is equal to 1 µV.

It can be deduced from Fig. 2 that specimens of identical size exhibit similar behaviour. Thus, the specimens with dimensions 100×100×400 mm^3 designated with the symbol v have a lower value of acoustic emission activity than the specimens with smaller dimensions, i.e. 40×40×160 mm^3 designated m. The strengths of all the monitored specimens are approximately the same – see Tab. 3.

The RMS values in Fig. 3. have been divided based on the size of the test specimens. A significant change in the acoustic emission activity in large specimens (see Fig. 3b) occurs from the compressive stress value of 20 MPa. In the case of smaller specimens (see Fig. 3a), the change is less evident but occurs again in the region of the compressive stress of 20 MPa.

In order to make the comparison of the change of the acoustic emission activity for the same specimens but of different dimensions clearer, the graphs in Fig. 4 have been created. The presented graphs clearly show a lower recorded acoustic emission activity for larger specimens.

Fig. 5 shows the number of recorded acoustic emission events (n) at a compressive stress (R), both cumulatively (Fig. 5a) and cumulatively relatively (Fig. 5b). Both graphs in Fig. 5 indicate a change in the activity at the knee regions of the curves, i.e. around 20 MPa. In addition, the recorded acoustic emission activity of the large specimens (designated $c - v$ and $o - v$) is lower than that of the small specimens (designated $c - m$ and $o - m$).

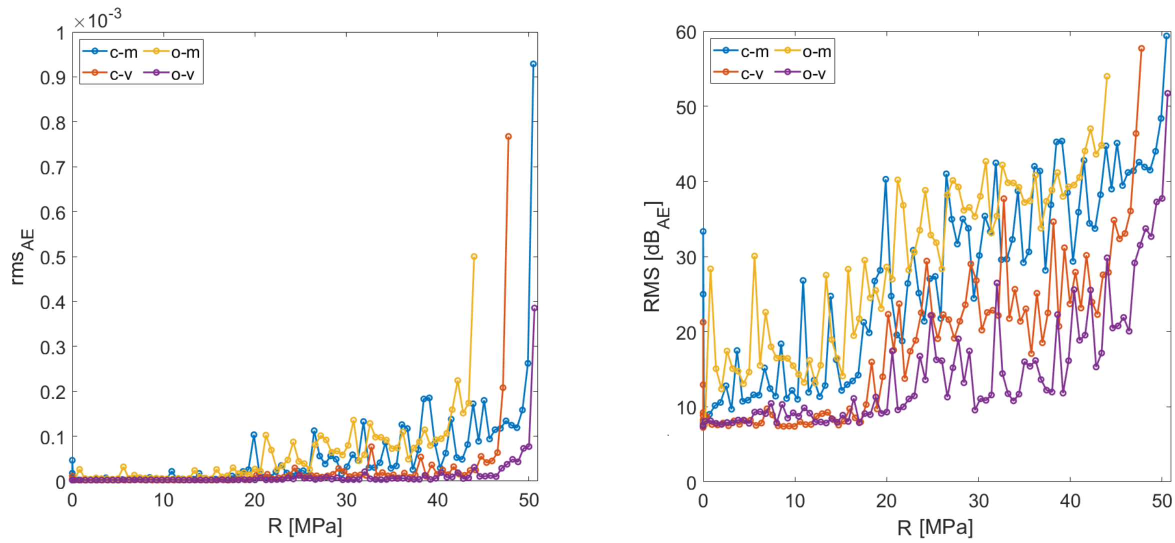

(a) RMS in a linear scale

(b) RMS in logarithmic (dB) scale

Fig. 2: The course of the RMS parameter for all types of specimens.

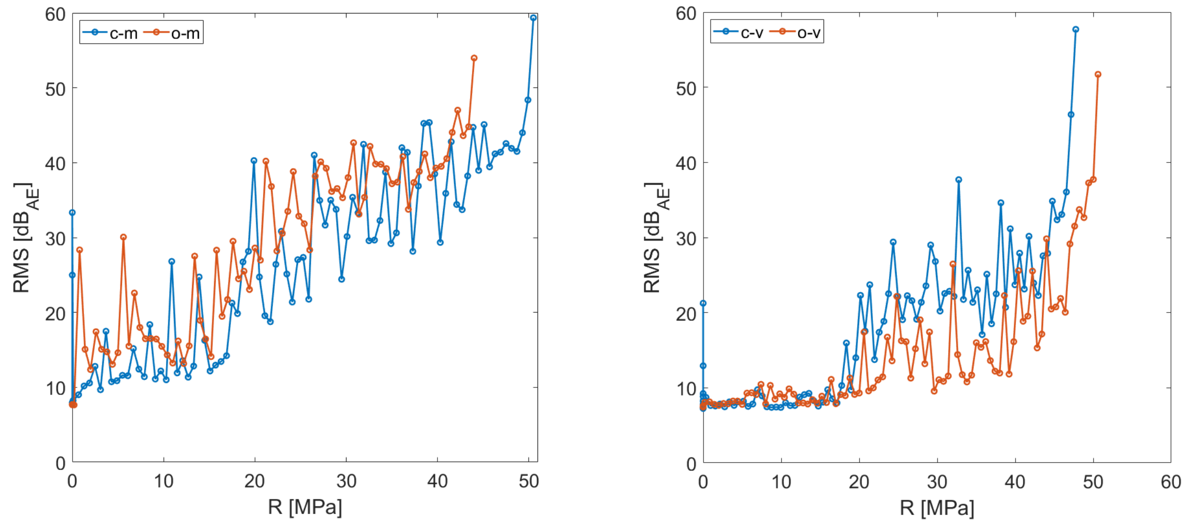

(a) Small specimens

(b) Large specimens

Fig. 3: The course of the RMS (in dB) parameter for individual sizes of specimens.

The frequency spectra in Fig. 6 and Fig. 7 presented in the 1/24 octave version indicate similar characteristics of all the measured acoustic emission events. Note that the upper graph shows the order of the recorded event (ns) on the horizontal axis, the frequency (f) on the vertical axis, and the relative spectrum with different colour intensity. The lower graph then shows the development of stress (R) for individual events (ns). It is obvious from the graphs that a significant monitored range is in the frequency range from 10 kHz to 1 MHz. Since the signal was sampled at 10 MHz, it also met the Nyquist's theorem. This means that the sampling frequency was more than twice as high as the frequency contained in the event signals.

There are two basic types of waves in materials: fast longitudinal and slower shear waves. Due to the wave components and their different propagation velocities, the shape of the waveform is also affected. AE signals of a shear origin tend to acquire longer durations since the main energy arrives later, while tensile or compressive signals acquire shorter durations and higher frequencies. The R_a value is defined as [8]

$$R_a = \frac{\text{rise time}}{\text{peak amplitude}} \tag{4}$$

and the average frequency f_r as [9]

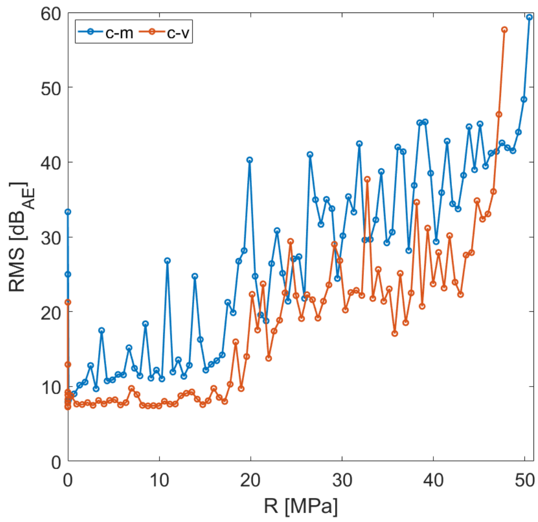

(a) Cement specimens of various sizes

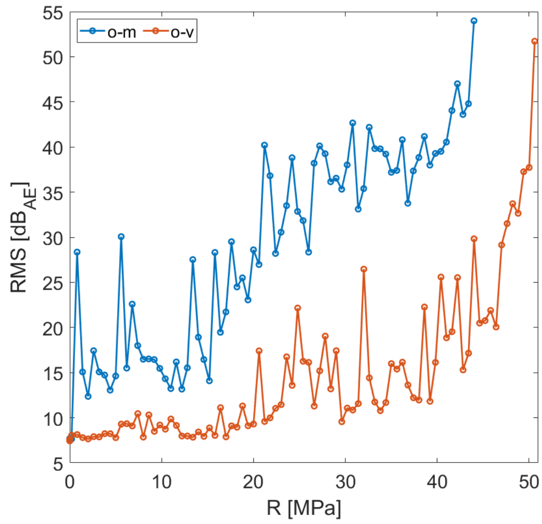

(b) Alkali-activated specimens of various sizes

Fig. 4: The course of the RMS (in dB) parameter for all types of specimens.

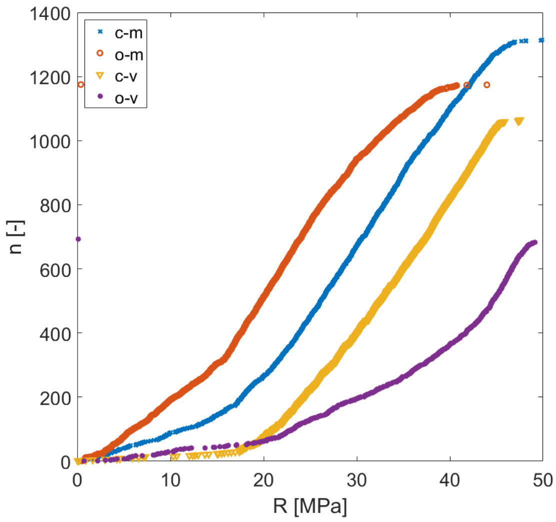

(a) Cumulative curves

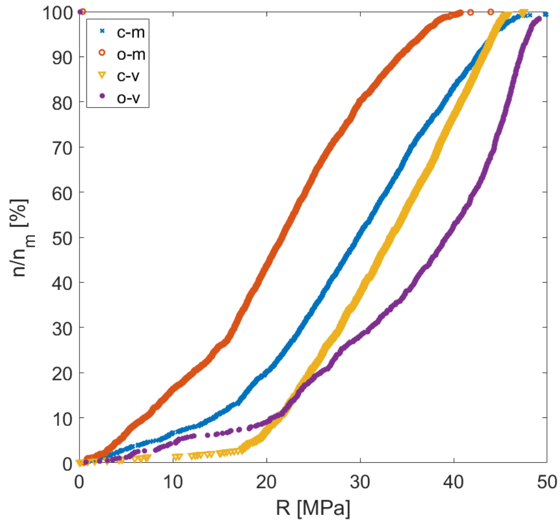

(b) Cumulative curves in relative

Fig. 5: Acoustic emission activity in the number of recorded events (n) depending on the pressure stress (R).

$$f_r = \frac{\text{ring down}}{\text{duration}} \,. \tag{5}$$

Fig. 8, Fig. 9, Fig. 10 and Fig. 11 then show the resolution of the compressive and shear stress. The 3D graphs in the figures designated a show the dependence of the R_a and f_r parameters on the development of compressive stress R. The 2D graphs in the figures designated b show a view from the direction of the pressure axis, i.e. the distribution of compressive and shear stresses determined by the acoustic emission method. The blue dots indicate the tensile stress and the red dots indicate the shear stress. The 2D graphs (b) also include a line separating the compressive and shear stresses. The shear stresses are therefore below the line. The presented graphs describing the pressure tests suggest that approximately 1/5 (20%) of the events originate in shear stresses. A comparison of Fig. 8a and, Fig. 9a with Fig. 10 and Fig. 11 clearly shows that a significant activity occurs in the compressive stress region above 20 MPa. However, in the case of smaller specimens, Fig. 8a and, Fig. 9a, the shear stress occurs earlier than in the case of large specimens Fig. 10a and Fig. 11a.

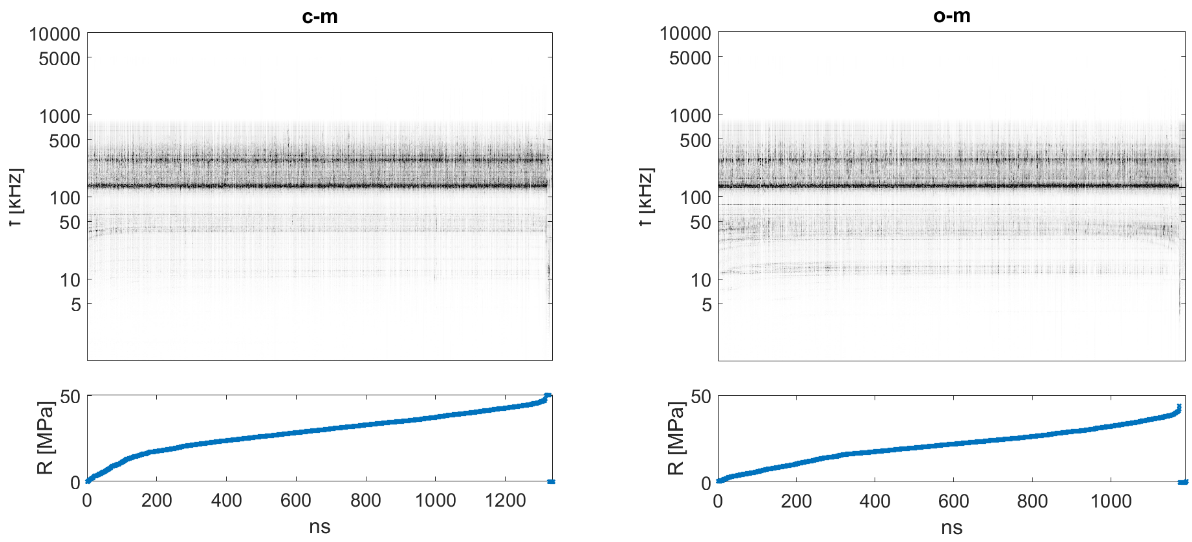

(a) Cement specimen (b) Alkali-activated specimen

Fig. 6: Frequency dependence of acoustic emission events in the case of small specimens.

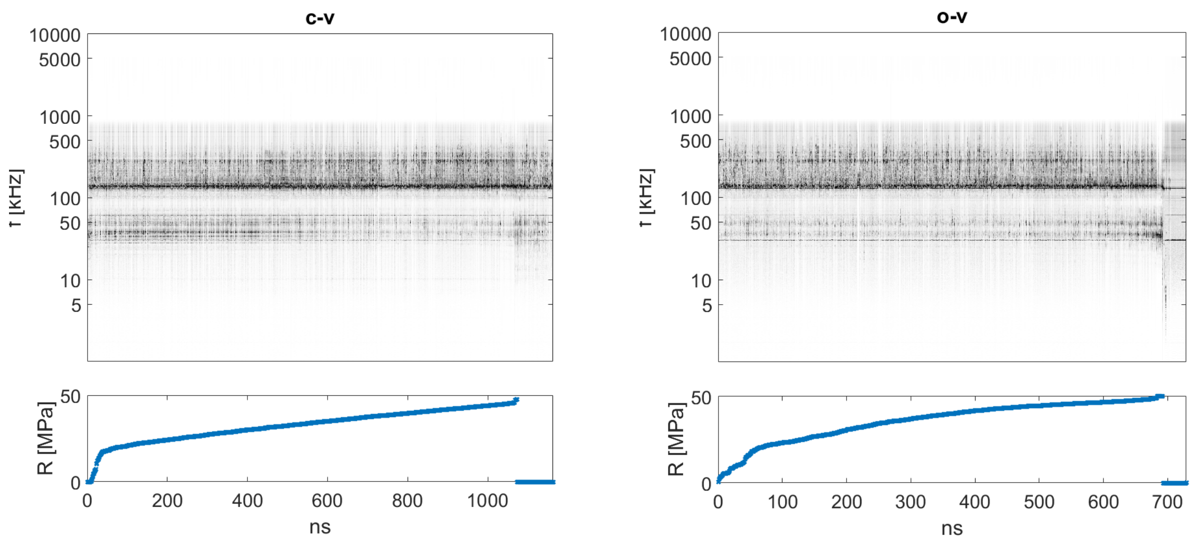

(a) Cement specimen (b) Alkali-activated specimen

Fig. 7: Frequency dependence of acoustic emission events in the case of large specimens.

4 Conclusion

The comparison of the mechanical properties of individual materials and test specimen sizes provided the following conclusions:

- with regard to compressive strength, the specimens produced from common mortar, i.e. cement mortar, reach approximately the same values as the specimens produced with the addition of alkali-activated slag;
- the results of the acoustic emission method follow a similar philosophy, i.e. there is no significant difference between the alkali-activated specimens and the specimens with common cement;
- of interest is the region around 20 MPa, where we start to see increased AE activity in larger samples that were “silent” up to this value.

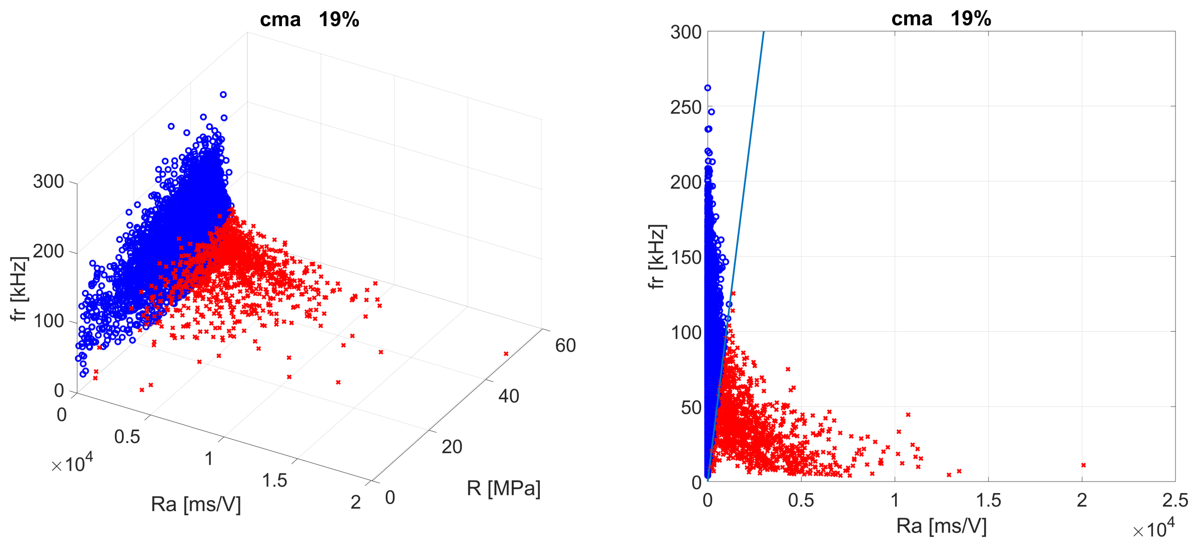

(a) 3D view (b) 2D view

Fig. 8: Probable distribution of compressive and shear stresses in a small cement specimen.

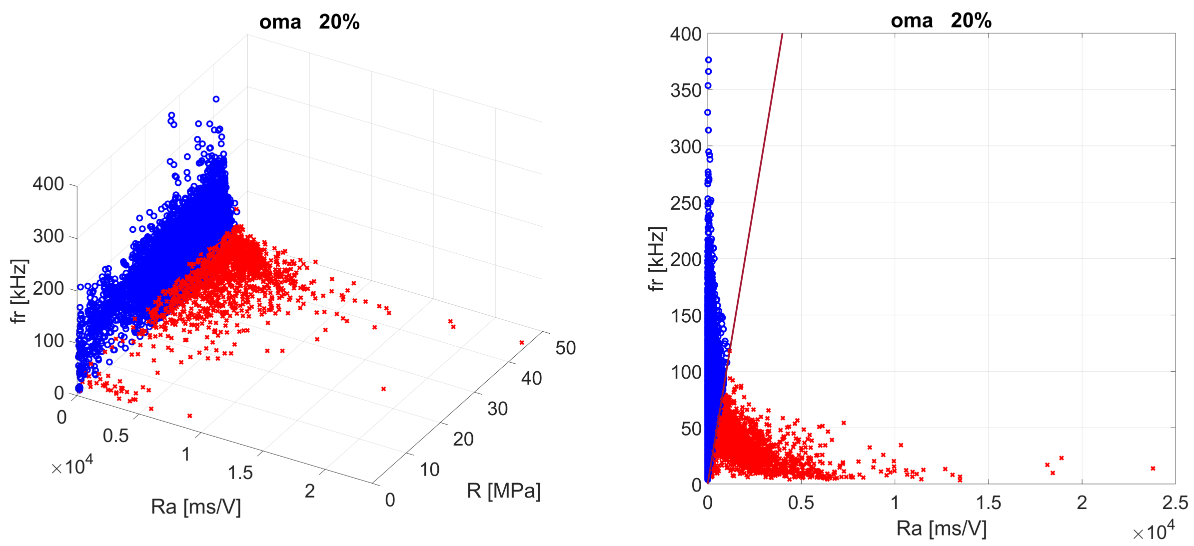

(a) 3D view (b) 2D view

Fig. 9: Probable distribution of compressive and shear stresses in a small alkali-activated specimen.

Acknowledgement

This paper has been worked out under the project Czech Science Foundation GACR No. GA 19-04703S "The use of non-destructive methods for testing of the condition of degraded alkaliactivated concrete" supported by Czech Science Foundation.

References

[1] L. Topolar, et al., Testing the Influence of the Material Bonding System on the Bond Strength of Large-Format Tiles Installed on Concrete Substrate under Mechanical Loading 13(14) (2020), doi: 10.3390/ma13143200.

[2] D. Kocab, et al., The analysis of acoustic emission signals detected during the loading of cement-based materials 99 (2019), 18–25, doi: 10.1016/j.engfailanal.2019.01.002.

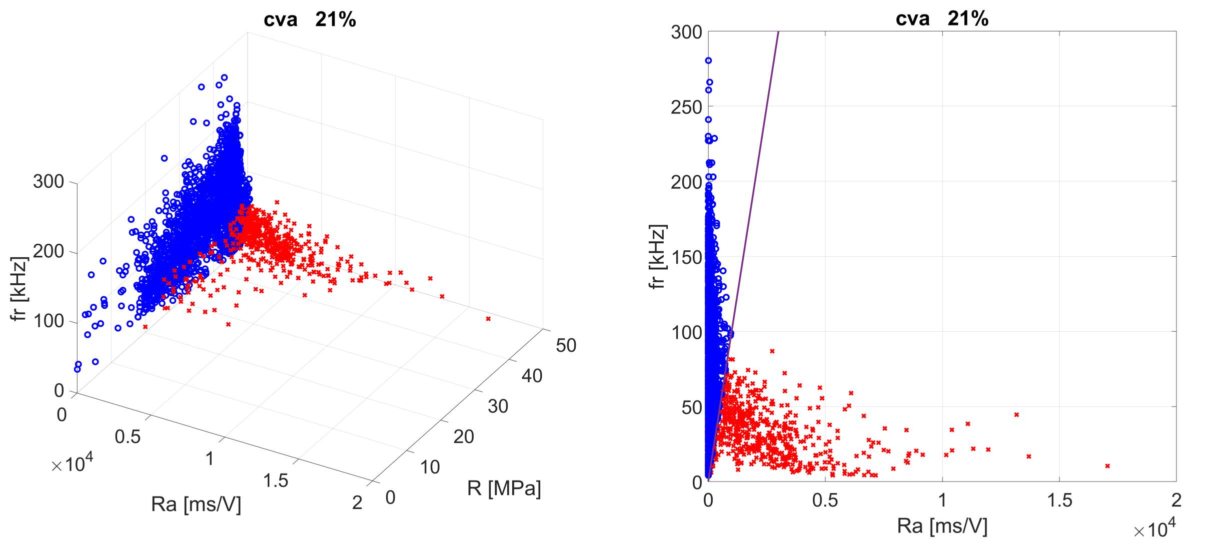

(a) 3D view (b) 2D view

Fig. 10: Probable distribution of compressive and shear stresses in a large cement specimen.

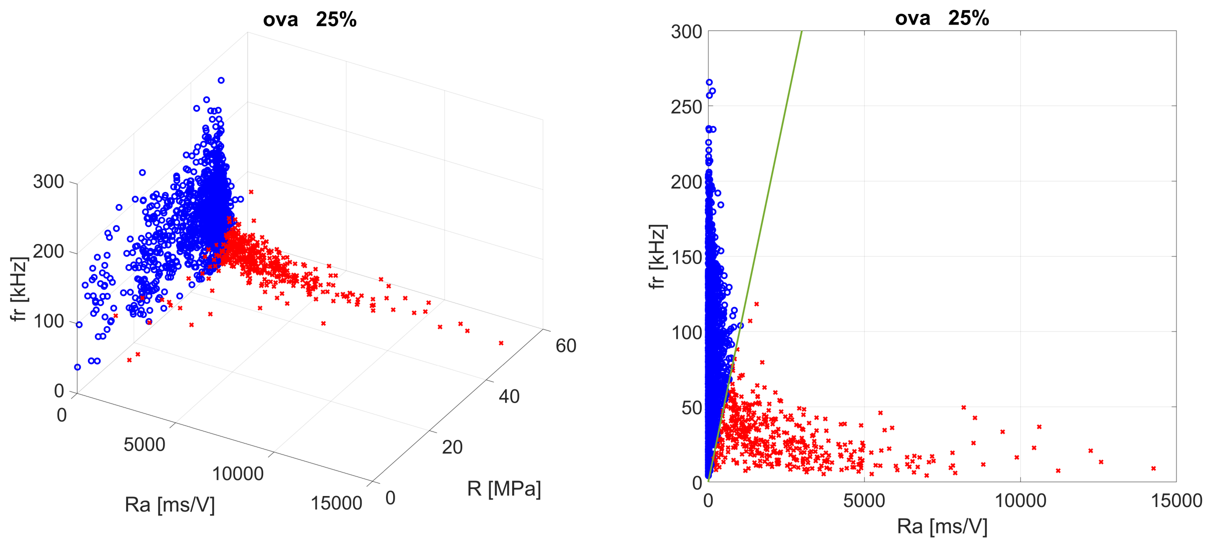

(a) 3D view (b) 2D view

Fig. 11: Probable distribution of compressive and shear stresses in a large alkali-activated specimen.

[3] D. Kocab, et al., Destructive and non-destructive assessment of the frost resistance of concrete with different aggregate, in proc.: 21st International Conference Building Materials, Products and Technologies (2018) Ceskovice Czech rep., doi: 10.1088/1757-899X/379/1/012022.

[4] D. Kocab, et al.: Development of the Elastic Modulus of Concrete under Different Curing Conditions, in proc.: 18th International Conference on Rehabilitation and Reconstruction of Buildings (2017), Brno Czech rep., 96–101, doi: 10.1016/j.proeng.2017.04.529.

[5] L. Topolar, et al.: The Acoustic Emission Parameters Obtained during Three-point Bending Test on Thermal-stressed Concrete Specimens, in proc.: 3rd International Conference on Structural and Physical Aspects of Construction Engineering, (2017) Slovakia, 111–117, doi: 10.1016/j.proeng.2017.05.315.

[6] B. Kucharczykova, et al.: Evaluation of Shrinkage, Mass Changes and Fracture Properties of Fine-aggregate Cement-based Composites during Ageing, in proc.: 3rd International Conference on Structural and Physical Aspects of Construction Engineering (2017) 357–364, doi: 10.1016/j.proeng.2017.05.349.

[7] L. Topolar, et al.: Applying method of acoustic emission for monitoring of different concrete mixture during setting and hardening, Solid State Phenomena (249) (2016) 91–95, doi: 10.4028/www.scientific.net/SSP.249.91.

[8] Y.X. Gan, et al.: Evaluation indexes of granite splitting failure based on RA and AF of AE parameters, Rock and Soil Mechanics (2020) 2324–2332, doi: 10.16285/j.rsm.2019.1460.

[9] Q.H. Han, et al.: Acoustic emission data analyses based on crumb rubber concrete beam bending tests, Engineering fracture Mechanics (210) (2019) 189–202, doi: 10.1016/j.engfracmech.2018.05.016.